Turkish Journal of Chemistry

http://journals.tubitak.gov.tr/chem/

Research Article

Turk J Chem
(2014) 38: 1013 – 1026

doi:10.3906/kim-1406-32

TD-DFT calculations and MCD spectroscopy of porphyrin and phthalocyanine analogues: rational design of photosensitizers for PDT and NIR region sensor applications

John MACK*, Martijn WILDERVANCK, Tebello NYOKONG
Department of Chemistry, Faculty of Science, Rhodes University, Grahamstown, South Africa

Received: 14.06.2014 • **Accepted:** 23.07.2014 • **Published Online:** 24.11.2014 • **Printed:** 22.12.2014

Abstract: Geometry optimizations and TD-DFT calculations have been carried out on series of fused-ring-expanded phthalonitriles, phthalocyanines, and aza-dipyrromethene boron difluoride (aza-BODIPY) dyes and trends in their optical and redox properties have been analyzed. The potential utility of fused-ring-expanded phthalocyanine and aza-BODIPY analogues for photodynamic therapy and near infrared region sensor applications is assessed on this basis. Recent attempts to prepare fused-ring-expanded aza-BODIPY analogues with benzene, pyrazine, and naphthalene rings have demonstrated that the properties of aza-BODIPYs vary markedly when different fused ring systems are added to the β-carbons of the pyrrole rings. A comparison of the TD-DFT calculations demonstrates that, as has previously been postulated, trends in the optical spectra, redox properties, and electronic structures of aza-BODIPYs follow those observed for the phthalonitrile precursors and the analogous phthalocyanines despite the absence of a fully conjugated macrocyclic perimeter that obeys Hückel's rule.

Key words: TD-DFT calculations, phthalocyanines, aza-BODIPYs

1. Introduction

There is considerable interest in the development of new generations of photosensitizers for photodynamic therapy (PDT), which absorb strongly in the therapeutic window between 650 and 1000 nm, where autofluorescence and absorption by water, tissues, and cells are minimized, and there is less light scattering. The first photosensitizer to be approved for use in PDT was Photofrin, a mixture of oligomers formed containing up to 8 porphyrin units linked by ether and ester bonds. The main drawback with Photofrin is that porphyrins absorb only weakly at the red end of the visible region, so high concentrations of the dye are required and this means that patients often remain sensitized to light for prolonged periods after each laser treatment. There has also been considerable interest in the use of organic dyes, which fluoresce in this region for intracellular imaging based on selectivity and sensitivity toward a specific ion.[1,2]

Several phthalocyanines (Pcs) have recently been approved for use in PDT, which absorb strongly at the red end of the visible region in the 660–690 nm range.[3,4] Although Pcs are very efficient photosensitizers, they are also far from ideal because their main absorption band lies at the edge of the therapeutic window. If photosensitizers could be developed that absorb strongly at the heart of the optical window, the utility of PDT-related therapies could be extended to deeper-lying tissues. Unfortunately, fused-ring-expansion of Pcs with benzene rings to form naphthalocyanine and anthracocyanine, the most obvious solution in this regard,

*Correspondence: j.mack@ru.ac.za

has been found to result in issues with compound stability, so new approaches will need to be adopted for this field of research to achieve its full potential.[5,6]

In recent years, there has been an increasing focus on the photophysical properties of dipyrromethene boron difluoride (BODIPY) dyes with red-shifted spectral bands, since heavy atoms can be introduced to enhance the rate of intersystem crossing and hence the singlet oxygen quantum yields.[7−10] Structural modifications, such as the incorporation of an aza-nitrogen atom to form aza-dipyrromethene (aza-BODIPY) dyes, extension of the π-conjugation system with styryl substituents and fused-ring-expansion at the β-pyrrole carbons, result in a significant red-shift of the main spectral bands towards the near infrared (NIR) region.[11,12] Recent attempts to prepare fused-ring-expanded aza-BODIPY analogues with benzene, pyrazine, and naphthalene rings by reacting the appropriate phthalonitrile precursor with a Grignard reagent have demonstrated that the properties of aza-BODIPYs can vary markedly when different fused ring systems are fused on the β-carbons of the 2 pyrrole ring moieties.[13,14] During a study of the optical and redox properties of aza-BODIPYs that were fused-ring-expanded with peripheral benzo and 2,3-naphtho moieties, it was postulated that trends in the optical properties of the corresponding Pcs and their phthalonitrile precursors can be used to predict the properties of the corresponding aza-BODIPY dyes.[13] In this paper, geometry optimizations and TD-DFT calculations have been carried out for 3 related series of fused-ring-expanded phthalonitriles, Pcs, and aza-BODIPY model compounds to test this hypothesis through a comparison of trends in their optical and redox properties. The potential utility of fused-ring-expanded Pc and aza-BODIPY analogues for photodynamic therapy and NIR sensor applications is also assessed on this basis.

2. Results and discussion

In 2005, Mack et al.[15] reported an analysis of trends predicted in DFT and TD-DFT calculations of 17 radially symmetric zinc porphyrinoids, which included several fused-ring-expanded Pc complexes, that were carried out with the B3LYP functional. The closed shell d^{10} configuration of the Zn(II) ion was selected since it results in a complete absence of metal to ligand and ligand to metal charge transfer bands above 300 nm, so that trends in the energies of the main $\pi \rightarrow \pi^*$ transitions can be readily compared. It was demonstrated that trends in the electronic absorption and magnetic circular dichroism (MCD) spectra and electronic structures could be readily accounted for by using Michl's perimeter model as a conceptual framework for the trends predicted in TD-DFT calculations.[16−19] Magyar and Tretiak[20] demonstrated that TD-DFT calculations tend to significantly underestimate the energies of charge transfer bands and concluded that the BHandHLYP functional with a 50% Hartree–Fock (HF) component provided the most accurate predictions for the energies of states with significant charge transfer character. In the present study, the Coulomb-attenuated exchange-correlation (CAM-B3LYP) functional was used to carry out the TD-DFT calculations, since it includes a long-range correction of the exchange potential, which incorporates an increasing fraction of HF exchange as the interelectronic separation increases, making it better suited for studying compounds where there is scope for significant charge transfer in the electronic excited states. Reimer and coworkers[21] demonstrated that calculations carried out with the BP86 and B3LYP functionals underestimate the energy of states associated with the $1b_{2u} \rightarrow 1e_g^*$ one-electron transition of free base porphyrins and their fused-ring-expanded analogues due to its significant charge transfer character and that more accurate predictions are provided for the higher-energy $\pi\pi^*$ states, which correspond more closely to experimental data, provided by TD-DFT calculations carried out with the CAM-B3LYP functional. Nemykin and coworkers[22] demonstrated that the analogous $1b_{2u}$ MO of zinc phthalocyanine also changes energy relative to the 4 key frontier π-MOs of Michl's perimeter model[16−19] based on the size of

the HF component used in the exchange-correlation functional and that this can have a significant impact on the accuracy of the calculated spectra.

In the context of Michl's perimeter model, a 16 atom 18 π-electron cyclic polyene corresponding to the inner perimeter of the porphyrinoid ligand can be used as a parent perimeter for describing and rationalizing the optical properties. The π-system contains a series of MOs arranged in ascending energy with $M_L = 0, \pm1, \pm2, \pm3, \pm4, \pm5, \pm6, \pm7$ and 8 nodal properties based on the magnetic quantum number for the cyclic perimeter, M_L. The highest occupied molecular orbital (HOMO) and lowest unoccupied molecular orbital (LUMO) have $M_L = \pm4$ and ±5 nodal properties, respectively. The 4 spin-allowed $M_L = \pm4 \rightarrow \pm5$ excitations give rise to 2 orbitally degenerate ^1E_u excited states, on the basis of the $\Delta M_L = \pm9$ and $\Delta M_L = \pm1$ transitions. The transitions to the $\Delta M_L = \pm9$ and ±1 excited states result in forbidden and allowed spectral Q and B bands of Gouterman's 4-orbital model,[23] since an incident photon can provide only 1 quantum of orbital angular momentum. Michl[16–19] introduced an **a**, **s**, **-a**, and **-s** terminology (Figure 1) for the 4 MOs derived from the HOMO and LUMO of the parent perimeter so that π-systems of porphyrinoids with differing molecular symmetry and relative orderings of the 4 frontier π-MOs in energy terms can be readily compared. One MO derived from the HOMO of a $C_{16}H_{16}^{2-}$ parent hydrocarbon perimeter and another derived from the LUMO have nodal planes that coincide with the yz-plane and are referred to, respectively, as the **a** and **-a** MOs, while the corresponding MOs with antinodes on the yz-plane are referred to as the **s** and **-s** MOs (Figure 1).

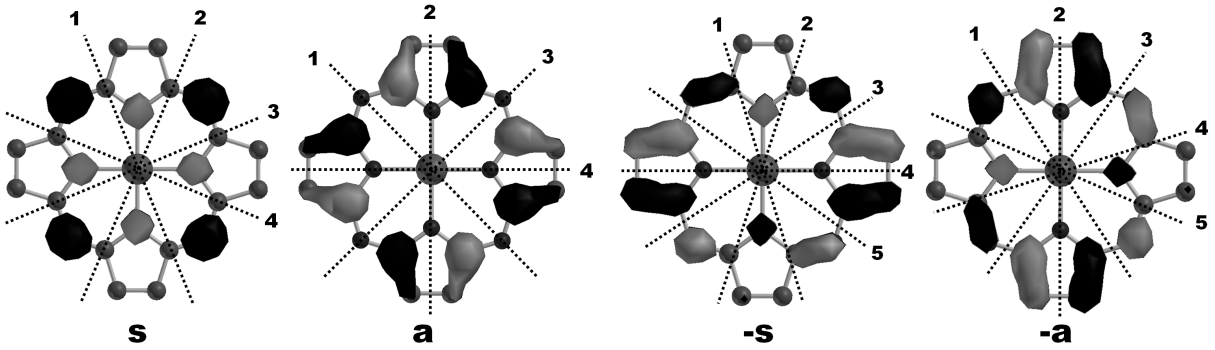

Figure 1. Nodal patterns of the 4 frontier π-MOs of zinc tetraazaporphyrin at an isosurface value of 0.04 a.u. Michl[16–19] introduced **a**, **s**, **-a**, and **-s** nomenclature to describe the 4 frontier π-MOs with $M_L = \pm4$ and ±5 nodal patterns based on whether there is a nodal plane (**a** and **-a**) or an antinode (**s** and **-s**) on the y-axis. Once the alignment of the nodal planes has been clearly defined, the effect of different structural perturbations can be readily conceptualized on a qualitative basis through a consideration of the relative size of the MO coefficients on each atom on the perimeter.

When TD-DFT calculations were carried out with the CAM-B3LYP functional on the B3LYP geometries of the Zn(II) complexes of porphyrin (**1**) and tetraazaporphyrin (**7**) and ligands that have been fused-ring-expanded with benzene (**2**, **8**), 2,3-naphthalene (**3**, **9**), anthracene (**4**, **10**), phenanthrene (**5**, **11**) and phenanthroline (**6**, **12**) moieties broadly similar trends are observed in the energies predicted for the energies of the Q bands and the HOMO–LUMO gaps (Figure 2; Table 1). There is a systematic overestimation of the energies of the Q and B bands as is normally observed in the TD-DFT calculations for porphyrinoids.[15] Series of tetraazaporphyrins with peripheral pyrazine (**13**–**17**) and benzopyrazine (**18**–**22**) moieties were also studied. As was observed previously with a similar set of calculations using the B3LYP functional,[15] when a comparison is made with experimentally observed values the TD-DFT calculations consistently overestimate the energy of the Q bands. In a similar manner to what has been reported in previous studies,[15,24] when benzo groups are

added to the ligand periphery of porphyrin (**1**) or tetraazaporphyrin (**7**) to form tetrabenzoporphyrin (**2**) or Pc (**8**), there is a narrowing of the predicted HOMO–LUMO gap in DFT and TD-DFT calculations (Figure 2) due to a destabilization of the **a** MO relative to the **s**, **-a**, and **-s** MOs. A similar effect is observed when the frontier π-MOs of naphthalocyanine (**9**) and anthracocyanine (**10**) are compared to those of Pc (**8**), but it is smaller in magnitude since the additional rings lie further from the inner perimeter where the largest MO coefficients are anticipated for the frontier π-MOs derived from the HOMO and LUMO of the parent perimeter (Figure 3). Benzo substitution has a destabilizing effect on the energy of the **a** MO because there is an antibonding interaction at the point of attachment of the C_4H_4 bridges that are added upon fused-ring-expansion and there are also nodal planes on the 4 aza-nitrogens and hence a smaller stabilization effect due to the electronegativity

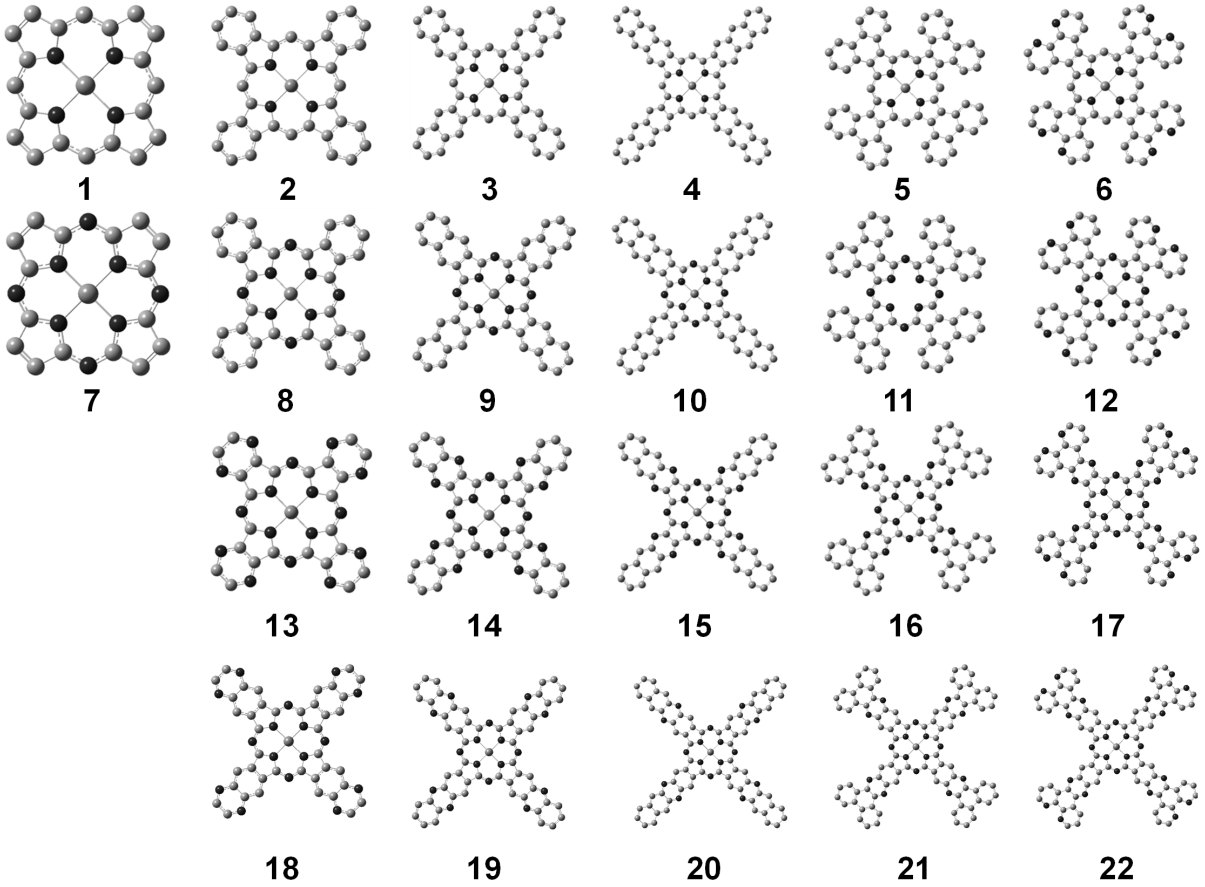

Figure 2. The MO energies predicted for the Zn(II) complexes of porphyrin (**1**), and its analogues fused-ring-expanded at the pyrrole β-carbons with benzene (**2**), 2,3-naphthalene (**3**), anthracene (**4**), phenanthrene (**5**), and phenanthroline (**6**) moieties, and the corresponding tetraazaporphyrins (**7**–**12**), β,β-tetrapyrazino-substituted tetraazaporphyrin (**13**), and its analogues fused-ring-expanded with benzene (**14**), 2,3-naphthalene (**15**), phenanthrene (**16**), and phenanthroline (**17**) moieties, and the corresponding β,β-tetrabenzopyrazino-substituted structures (**18**–**22**). Bolder black lines are used to highlight the 4 frontier π-MOs that are associated with Michl's perimeter model.[16–19] Black triangles and circles are used to denote the **a** and **s** MOs, respectively. Large gray diamonds and small gray triangles and circles are used to plot the predicted HOMO–LUMO gaps and the predicted and observed Q band energies, respectively, against a secondary axis. Horizontal lines are used to highlight the HOMO energies of the Zn(II) complexes of phthalocyanine (**8**) and naphthalocyanine (**9**), so that the relative stabilities of the other compounds can be assessed.

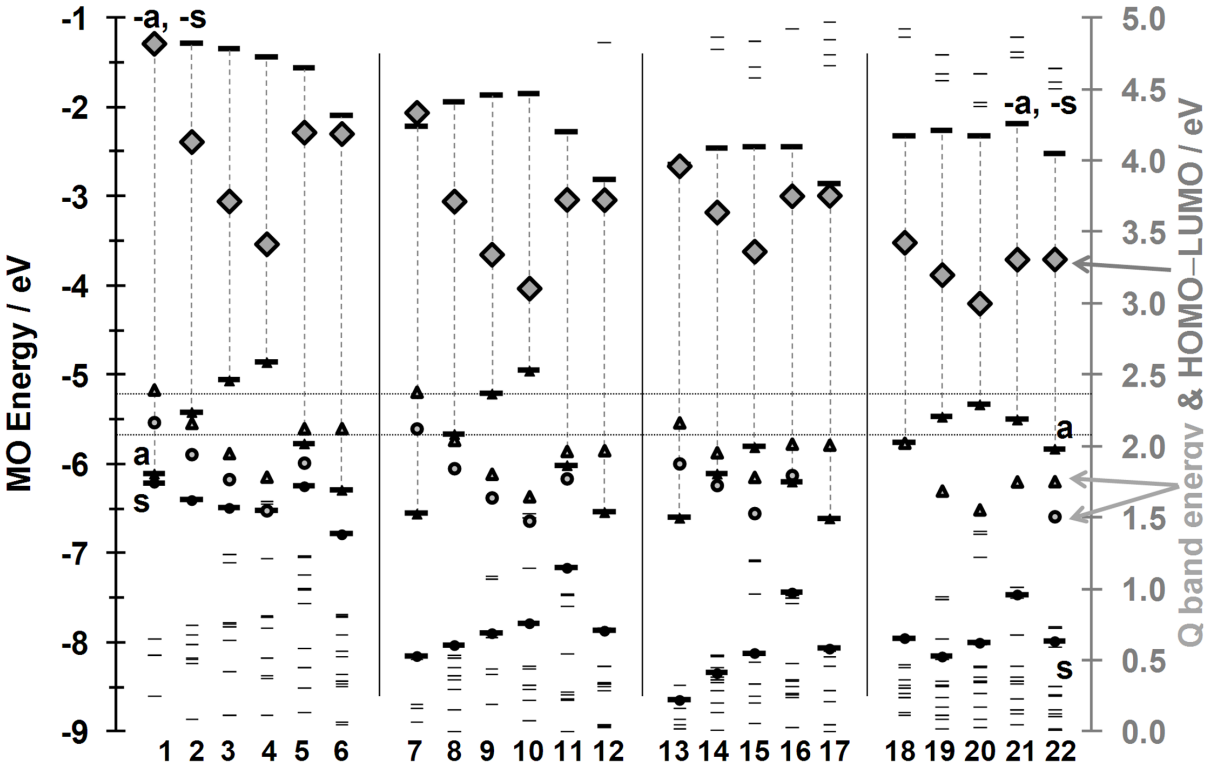

Figure 2. Continued.

of these atoms. Since the HOMO is destabilized, there is a decrease in the first oxidation potential and hence in the stability of the compounds with respect to oxidative attack. Kobayashi and coworkers[6] used theoretical calculations and spectroscopic measurements to demonstrate that this makes most anthracocyanine (**10**) complexes unstable.

Table 1. Predicted and observed Q band wavelengths (λ, nm) and calculated oscillator strengths (f) for the series of fused-ring-expanded Zn(II) porphyrins, tetraazaporphyrins, and their radially symmetric tetrapyrazino- and tetrabenzopyrazino- analogues.

	λ_{calc}	f_{calc}	λ_{exp}	Ref.		λ_{calc}	f_{calc}	λ_{exp}	Ref.
1	517	0.01	572[a]	46	**12**	629	0.45	—	—
2	573	0.20	638	47	**13**	572	0.38	660[b]	30
3	636	0.43	701	48	**14**	634	0.57	718	31
4	694	0.58	800	49	**15**	695	0.73	810	30
5	583	0.12	658	50	**16**	615	0.65	690[c]	33
6	583	0.13	—	—	**17**	617	0.55	—	—
7	521	0.19	584[a]	51	**18**	613	0.65	—	—
8	607	0.48	672	52	**19**	734	0.77	—	—
9	686	0.72	756	53	**20**	796	0.79	—	—
10	752	0.91	839	6	**21**	707	0.94	—	—
11	631	0.44	699[a]	24	**22**	707	0.92	822[b]	41

[a] – Mg(II) complex. [b] – free base compound. [c] – $SiCl_2$ complex.

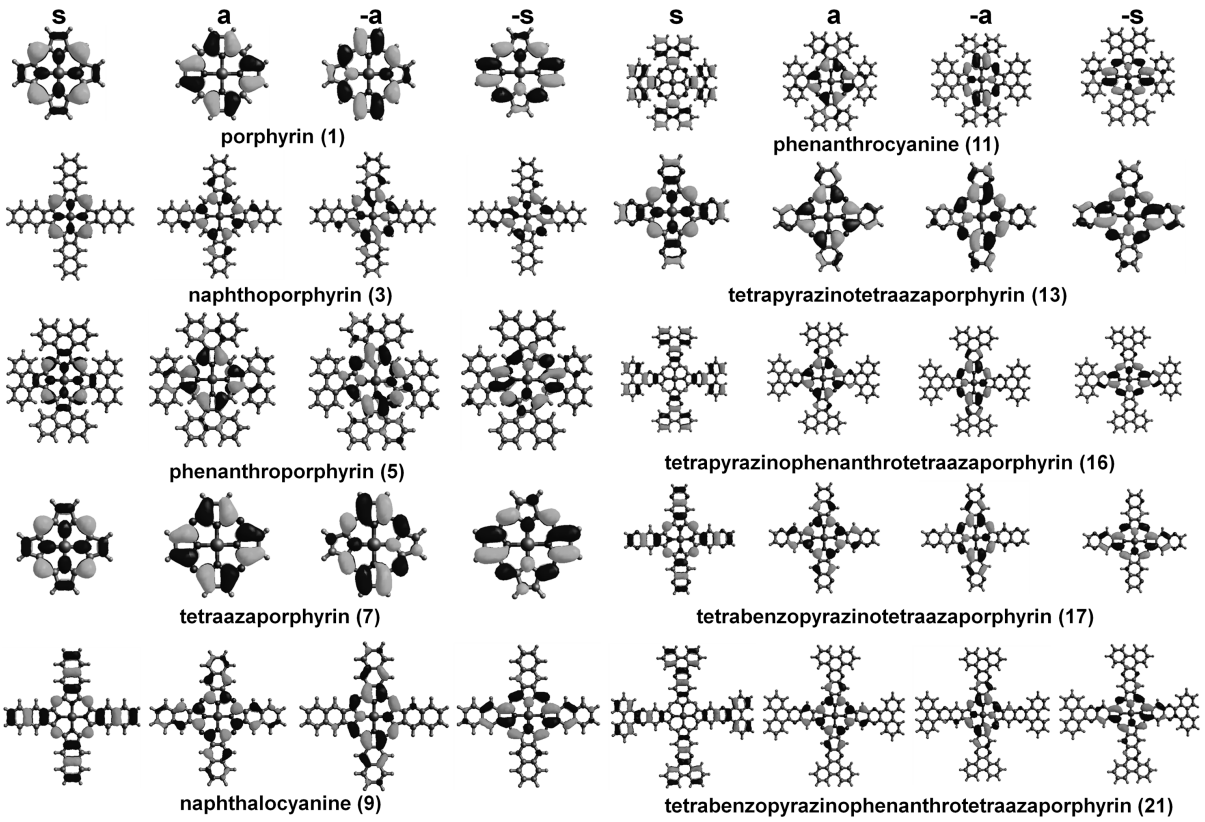

Figure 3. The nodal patterns of the frontier π-MOs of a series of fused-ring-expanded porphyrinoids at an isosurface value of 0.02 a.u.

Although radially symmetric fused-ring-expansion with benzene rings is problematic from the standpoint of compound stability, there is scope for forming fused-ring-expanded Pc analogues with other types of peripheral fused rings. Recent research by Shen and Mack and coworkers[25,26] has pointed the way to a possible solution based on using other types of fused ring systems such as phenanthrenes, since the alignment of the nodal planes on the peripheral fused rings differ markedly from those of benzo-fused analogues (Figure 3). In the context of porphyrin analogues,[24–26] the incorporation of phenanthrene moieties has been shown to result in significant red shifts of the main spectral bands due to a stabilization of the LUMO rather than a destabilization of the HOMO. Although similar trends are predicted for the corresponding Pc analogues (Figure 2), the wavelength of phenanthracocyanine (**11**)[27] lies only ca. 30 nm to the red of that of Pc (**8**) (Table 1). A limited amount of research has been carried out on tetraazaporphyrins that are fused-ring-expanded with perylene[28] and triphenylene[29] moieties at the β-carbons of the pyrrole moieties, but the Q bands have also been reported to lie at the red end of the visible region, so there is no obvious major advantage for NIR region applications. In the late 1960s, the Luk'yanets group[30,31] pioneered the introduction of novel fused-ring systems with peripheral pyrazine moieties. Subsequently, research was also carried out by the van Lier group on tetraazaporphyrin analogues with 1,2-naphthalene and pyrazinophenanthrene (**16**) moieties.[32,33] Pyrazino-fused tetraazaporphyrins have also recently been studied in depth by the Zimcik[34–37] and Faust[38–40] groups. The presence of the 8 additional electronegative nitrogen atoms in compounds **13**–**17** has a stabilizing effect on the frontier π-MOs and hence addresses the issue of compound stability, but there is a blue shift of the Q band relative to the comparable Pc analogues (**8**–**12**) (Figure 2; Table 1).

In 2002, Pilkington and coworkers reported the synthesis of a novel Pc analogue fused-ring-expanded with benzopyrazinophenanthroline moieties (**22**).[41] Although the presence of the additional set of benzene rings results in a further relative destabilization of the **a** MO (Figure 2), the energy of the HOMO remains comparable to that of the corresponding Pc (**8**) complex. The Q band was reported to lie at ca. 820 nm, in the center of the therapeutic window, but significant issues were encountered with solubility due to the π-π stacking properties of the planar ligands and that has limited subsequent research in this area. The results of the TD-DFT calculations demonstrate that there is scope for shifting the Pc Q band to wavelengths beyond 800 nm that are comparable to that of anthracocyanine (**4**) (Figure 2), in a manner that does not result in a significant destabilization of the HOMO if the problems encountered with solubility can be successfully addressed. The very intense Q band of Pc is retained in this context (Figure 4), since there is a large separation of the **a** and **s** MOs (referred to as the ΔHOMO value in the context of Michl's perimeter model[16–19]), due to the contrasting effects of the large MO coefficients of the **s** MO and angular nodal planes of the **a** MOs on the electronegative aza-nitrogen atoms. This results in a significant mixing of the allowed and forbidden properties of the B and Q bands, since there are no longer comparable contributions from one-electron transitions from the **a** and **s** MOs to the doubly degenerate LUMO in the Q and B excited states.

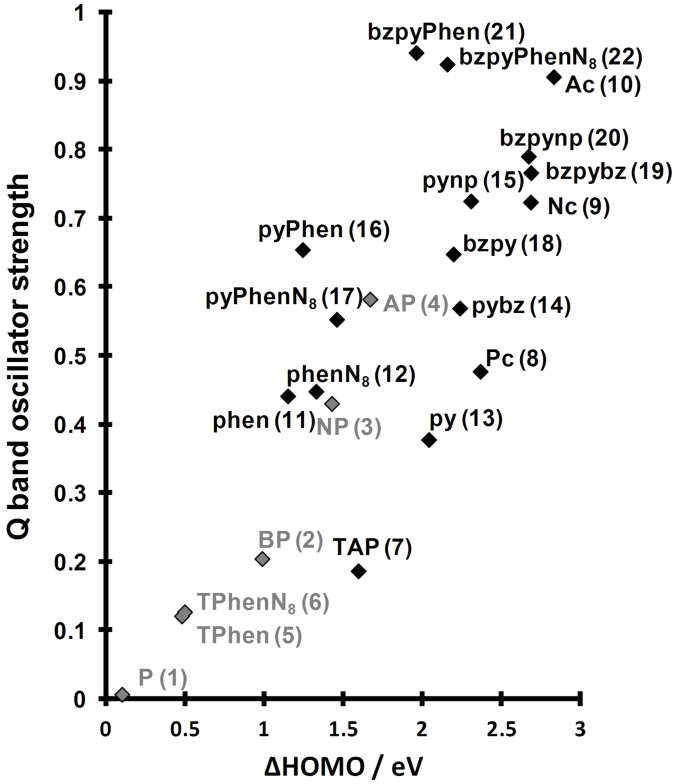

Figure 4. The predicted oscillator strength values for the series of Zn(II) porphyrin and tetraazaporphyrin analogues.

It has been postulated that the trends observed for the optical properties of aza-BODIPY dyes are likely to be similar to those of the corresponding tetraazaporphyrins[14] (Figures 2 and 5; Tables 1 and 2), despite the absence of a cyclic perimeter that formally fits Hückel's rule for aromaticity. BODIPY dyes can be viewed as being structural analogues of the porphyrins and have been the focus of considerable research interest in recent decades, due to their favorable photophysical properties, such as their high molar absorption coefficients,

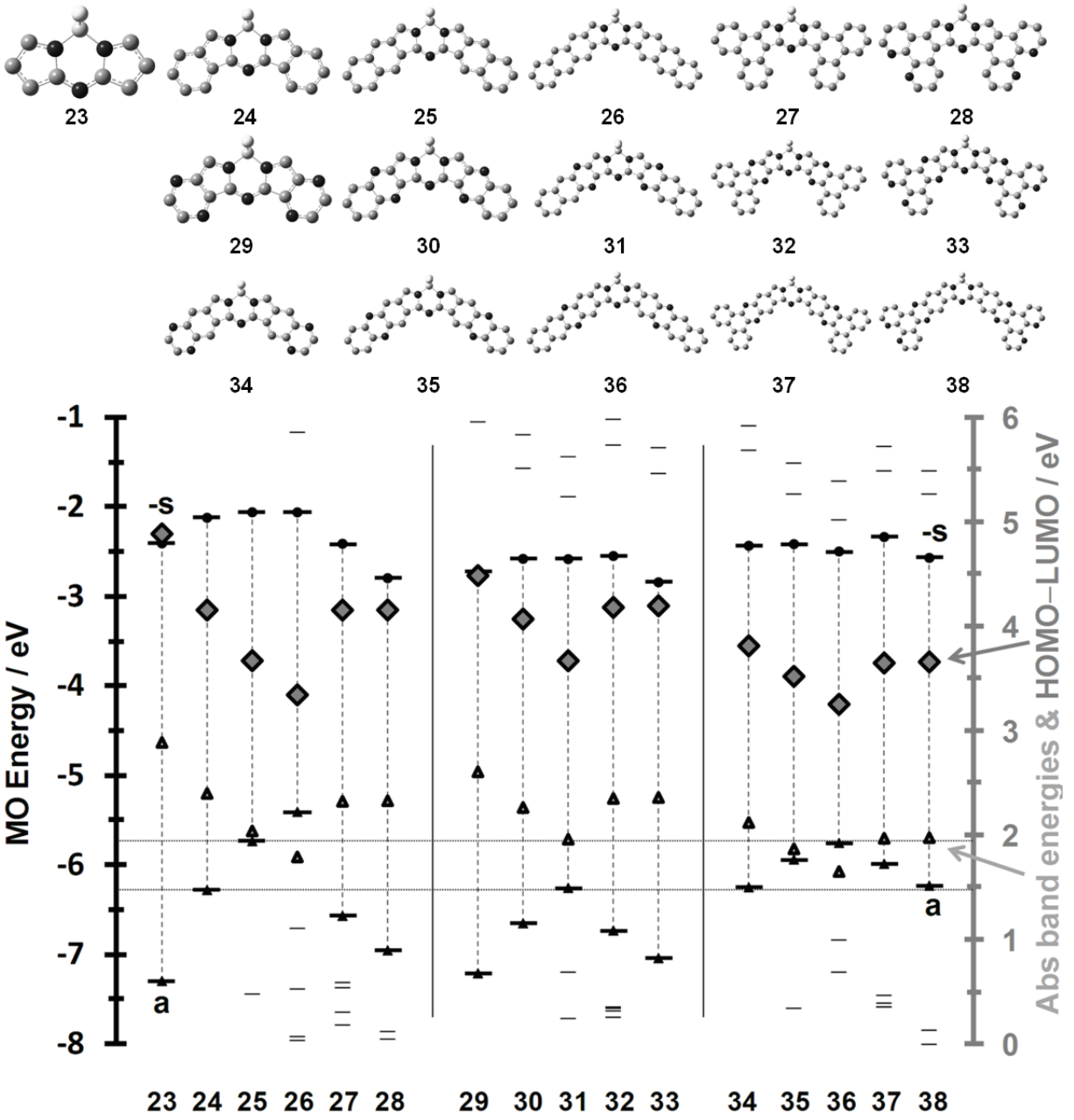

Figure 5. The MO energies predicted for the Zn(II) complexes of aza-BODIPY (**23**), and analogues fused-ring-expanded at the pyrrole β-carbons with benzene (**24**), 2,3-naphthalene (**25**), anthracene (**26**), phenanthrene (**27**), and phenanthroline (**28**) moieties, and β,β-tetrapyrazino-substituted aza-BODIPY (**29**), and structural analogues fused-ring-expanded with benzene (**30**), 2,3-naphthalene (**31**), phenanthrene (**32**), and phenanthroline (**33**) moieties, and the corresponding β,β-tetrabenzopyrazino-substituted structures (**34**–**38**). Bolder black lines are used to denote the HOMO and LUMO, which can be regarded as being analogous to **a** and **-s** MOs of Michl's perimeter model,[16−19] respectively, even in the absence of a fully conjugated cyclic perimeter. Large gray diamonds and small gray triangles are used to plot the predicted HOMO–LUMO gaps and lowest energy absorption bands against a secondary axis. Horizontal lines are used to highlight the HOMO energies of the benzo- (**24**) and 2,3-naphtho- (**25**) fused aza-BODIPYs, so that the relative stabilities of the other compounds can be assessed.

narrow absorption and emission bands, small Stokes shifts, and excellent photostability. MO calculations have demonstrated that there is a marked red-shift of the main spectral bands of aza-BODIPY dyes, since the LUMO has a large MO coefficient on the aza-nitrogen atom and this results in a marked narrowing of the HOMO–LUMO gap relative to the analogous BODIPYs (Figure 6).[11] The most important optical and photophysical properties of BODIPY dyes are retained, and so these compounds are potentially suitable for use in biomedical applications in the biological window. In a similar manner to what has been reported for fused-ring-expanded Pc analogues (Figures 2 and 3), significant issues were encountered with compound stability when 2,3-naphtho moieties were introduced at the pyrrole β-carbons.[13]

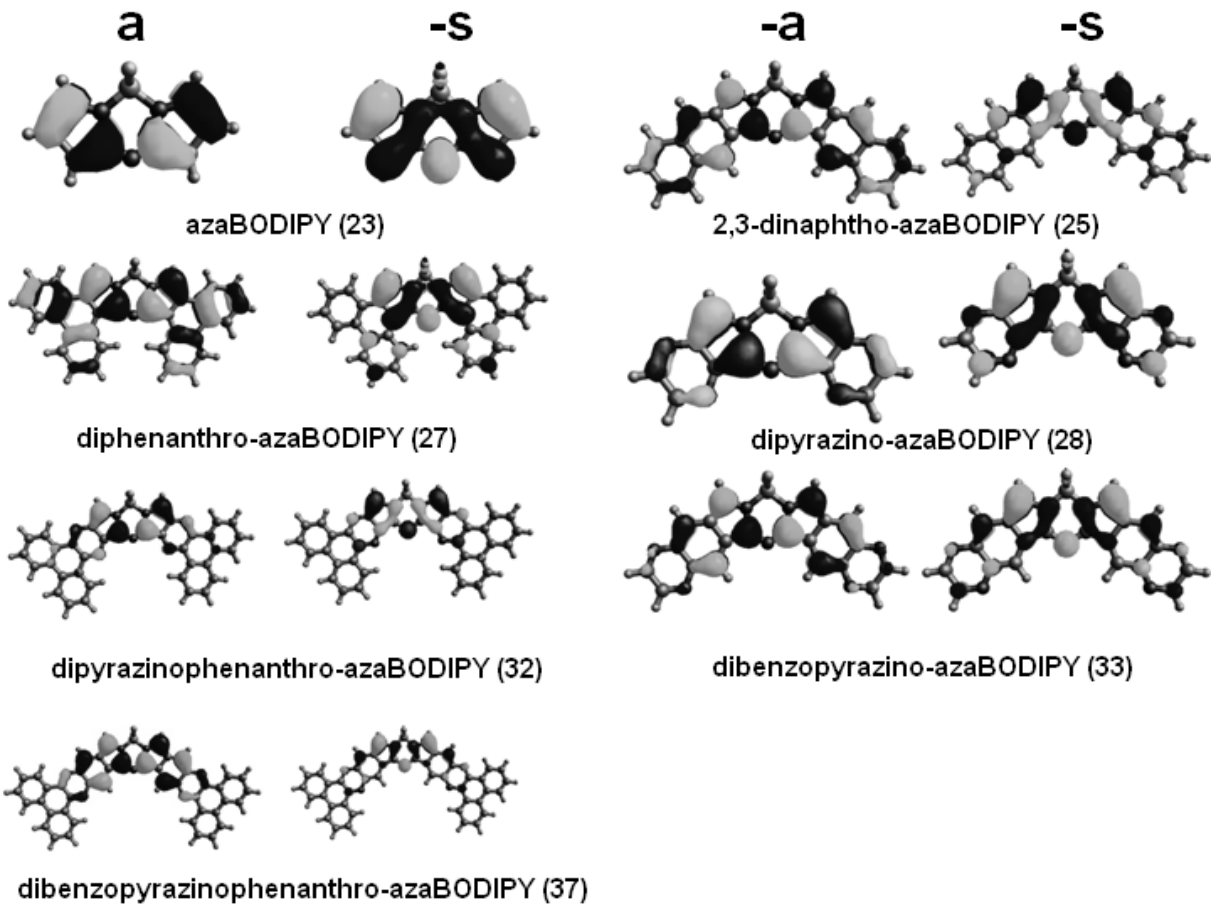

Figure 6. The nodal patterns for the frontier π-MOs of a series of fused-ring-expanded aza-BODIPYs at an isosurface value of 0.03 a.u.

Although aza-BODIPY dyes do not formally fit Hückel's rule for aromaticity, their properties are broadly similar to those of an aromatic π-system, since the coordination of the boron atom holds the dipyrromethene ligand in a rigidly planar conformation. The π-MOs associated with the indacene plane of BODIPYs can be compared to those of an aromatic $C_{12}H_{12}^{2-}$ cyclic perimeter, which has MOs arranged in a $M_L = 0, \pm1, \pm2, \pm3, \pm4, \pm5, 6$ sequence in ascending energy terms.[11] Although broadly similar angular nodal pattern sequences can be observed in the π-MOs of the BODIPY π-system, the introduction of the BF_2 moiety, cross links, and pyrrole nitrogen atoms results in a HOMO and a LUMO (Figures 5 and 6), which are well separated in energy

Table 2. Predicted wavelengths and oscillator strengths for the series of fused-ring-expanded aza-BODIPYs.

	λ_{calc}	f_{calc}		λ_{calc}	f_{calc}
23	429	0.44	**31**	631	0.72
24	516	0.75	**32**	570	0.73
25	607	0.92	**33**	563	0.75
26	691	0.99	**34**	583	0.83
27	533	0.90	**35**	662	0.74
28	531	0.91	**36**	749	0.59
29	475	0.66	**37**	628	1.11
30	547	0.73	**38**	626	1.07

terms from the other π-MOs of the dipyrromethene π-system. These MOs are comparable to the **a** and **-s** MOs of the analogous tetraazaporphyrins (Figure 4) in the manner in which the nodal planes are aligned with respect to the main 2-fold axis of symmetry that is associated with the *zy*-mirror plane. Theoretical calculations predict that the lowest-lying $S_0 \rightarrow S_1$ transition is associated almost exclusively with the HOMO $\rightarrow$ LUMO transition.[11] The effects of fused-ring-expansion on the wavelength of the lowest energy absorption band (Figure 5 and Table 2) are predicted to be similar to what is predicted for the analogous tetraazaporphyrins, since the alignment of the nodal planes of the frontier π-MOs is broadly similar (Figures 3 and 6). Comparatively few aza-BODIPYs have been studied and aryl substituents have tended to be introduced at the β-pyrrole carbons, which have a significant effect on the energies of the frontier π-MOs, so it is difficult to compare the calculated results to experimentally observed values. It should be noted, however, that when DFT and TD-DFT calculations were carried out for a series of BODIPY and aza-BODIPY dyes,[11] a systematic overestimation of the energies of the lowest energy absorption band was predicted, which is similar to that observed in the calculations for porphyrins and tetraazaporphyrins in Figure 2. It is reasonable to anticipate, therefore, that the trends in the predicted band energies would be reflected in the experimental values if compounds **23**–**38** were to be synthesized.

The HOMO of the aza-BODIPY π-system is directly comparable to that of the **a** MO of tetraazaporphyrins, since it also has nodal planes on the bridging aza- and pyrrole nitrogens. This means that the effect of incorporating fused-ring moieties and pyrazine nitrogens is broadly similar in both cases (Figures 2 and 5), and the qualitative predictions of the effect of structural modifications on the energies of the HOMO that have been made in the context of porphyrinoids can be readily extended to aza-BODIPYs. The trend in the energy of the LUMOs is also broadly similar to that observed for the analogous fused-ring-expanded tetraazaporphyrins. The reasons for this are not as immediately obvious, but in the context of the fused-ring-expanded tetraazaporphyrins it should be noted that the nodal patterns of the **-a** and **-s** MOs are rotated by 90° with respect to each other (Table 1) due to the $M_L = \pm 5$ orbital angular momentum properties of the LUMO of the parent high-symmetry hydrocarbon perimeter. Since aza-BODIPYs have 2 pyrrole moieties linked by an aza-nitrogen atom and have 2-fold symmetry with respect to the main symmetry axis, the analogy that can be made is with the nodal patterns of the 2 opposite pyrrole moieties of the **-s** MO, which has a large MO coefficient on the aza-nitrogens that lie on the *y*-axis (Figure 1).

The trends in the MO energies of the frontier π-MOs and in the HOMO–LUMO gaps of the analogous set of fused-ring-expanded phthalonitriles (**39**–**54**), shown in Figure 7, are also broadly similar to those predicted for the corresponding Pc (**1**–**22**) and aza-BODIPY (**23**–**38**) analogues. The alignments of the nodal planes of the **a** and **s** MOs (Figure 8) are similar to those of the corresponding tetraazapophyrin analogues (Figure 3),

as would be anticipated based on their radial symmetry and the manner in which the 4 angular nodal planes lie on alternating sets of 8 atoms on the inner perimeter due to the $M_L = \pm 4$ properties. The overall trend in the HOMO–LUMO gap does not follow that of the corresponding tetraazaporphyrins as closely as the trend for aza-BODIPYs does, since the absence of a 4-fold symmetry axis breaks the degeneracy of the **-a** and **-s** MOs (Figures 2 and 7).

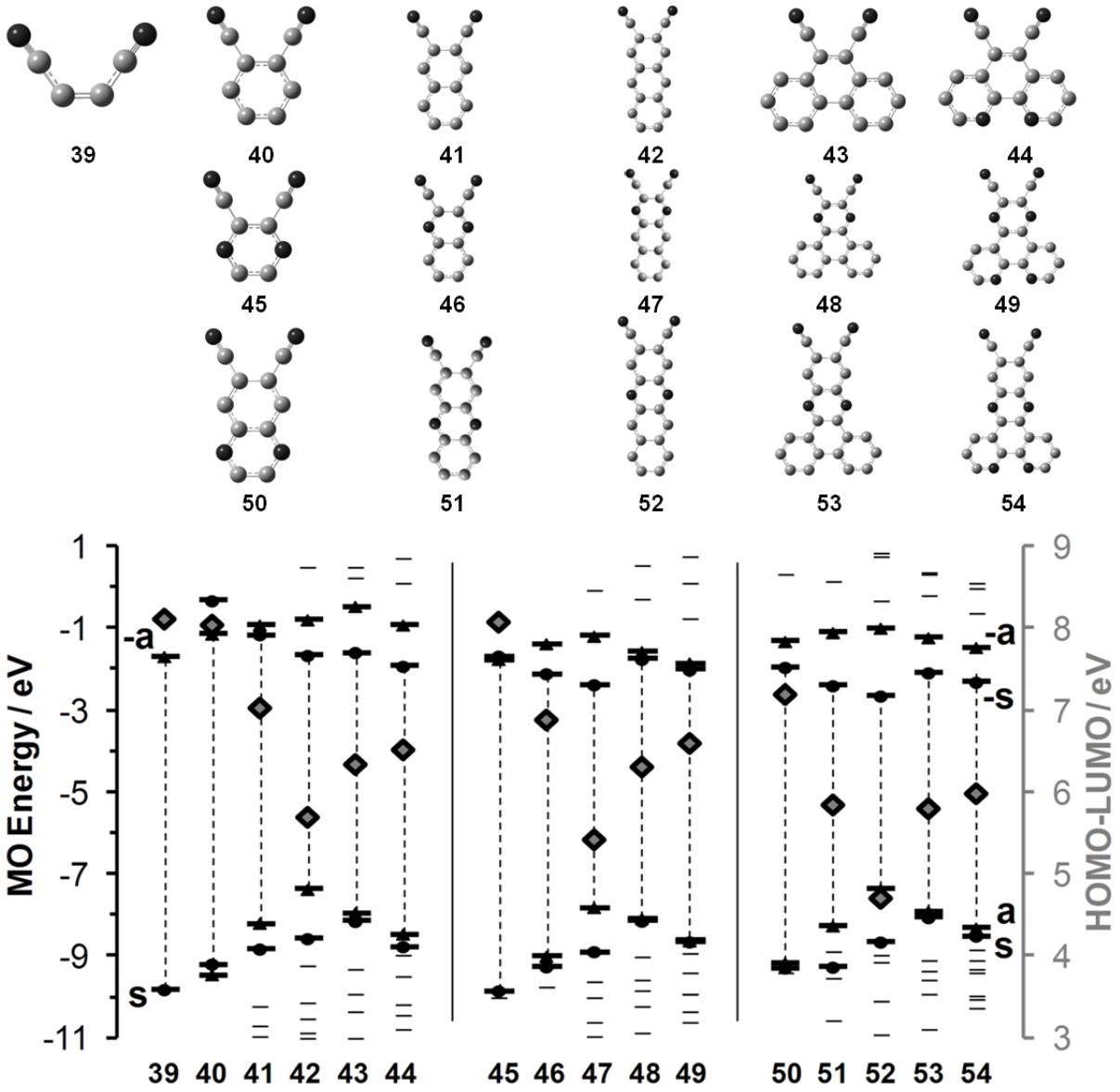

Figure 7. The MO energies predicted for maleonitrile (**39**), phthalonitrile (**40**), and structural analogues fused-ring-expanded at the pyrrole β-carbons with benzene (**41**), 2,3-naphthalene (**42**), phenanthrene (**43**), and phenanthroline (**44**) moieties, and β,β-tetrapyrazino-substituted phthalonitrile (**45**), and analogues fused-ring-expanded with benzene (**46**), 2,3-naphthalene (**47**), phenanthrene (**48**), and phenanthroline (**49**) moieties, and the corresponding β,β-tetrabenzopyrazino-substituted structures (**50**–**54**). Bolder black lines are used to highlight the 4 frontier π-MOs that are associated with Michl's perimeter model.[16–19] Black triangles and circles are used to denote the **a/-a** and **s/-s** MOs, respectively. Gray diamonds are used to plot the predicted HOMO–LUMO gaps against a secondary axis.

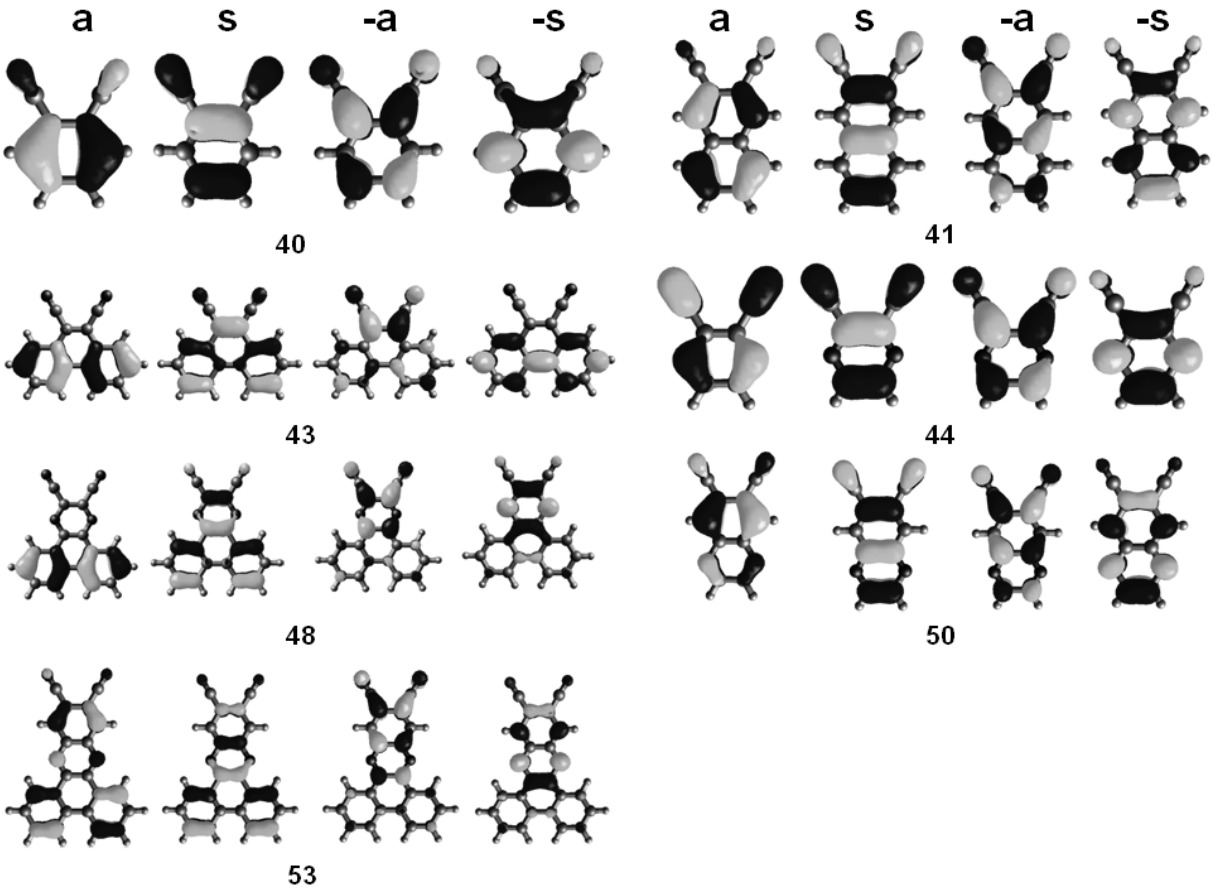

Figure 8. The nodal patterns for the frontier π-MOs of a series of fused-ring-expanded phthalonitriles at an isosurface value of 0.02 a.u.

The similarity of the trends observed in the predicted MO energies and Q band energies for the series of analogous fused-ring-expanded tetraazaporphyrins and aza-BODIPYs and to a lesser extent the corresponding phthalonitriles (Figures 2, 5, and 7) clearly demonstrates that, as has been postulated previously,[13] the trends in the wavelengths of the lowest-energy spectral bands of both phthalonitriles and Pcs can reasonably be used as a guide as to whether the corresponding aza-BODIPY compound is likely to have an intense spectral band that is shifted significantly into the NIR region. The trends in compound stability that are related to the first oxidation potential that have been investigated in the context of Pc analogues[6] are also likely to be observed in the context of the corresponding aza-BODIPYs. Although the aza-BODIPY π-system lacks a fully conjugated macrocycle perimeter, the rigid planar geometry associated with the coordination by a BF_2 moiety results in frontier π-MOs with nodal patterns that are broadly similar to those of the corresponding Pcs, so a qualitative perimeter model approach to predicting the energies of the frontier π-MOs can still be applied. The identification of these trends should facilitate research on the use of aza-BODIPY analogues in PDT and bioimaging related applications. Research on complexes containing BODIPY and Pc moieties may also be facilitated.[42–44]

3. Experimental

Geometry optimization calculations were carried out for 22 porphyrins and tetraazaporphyrins and 16 aza-BODIPY and phthalonitrile structures using the B3LYP functional of the Gaussian09 software packages[45] with

6-31G(d) basis sets. The B3LYP optimized geometries were used to carry out TD-DFT calculations using the CAM-B3LYP functional with 6-31G(d) basis sets.

Acknowledgment

The theoretical calculations were carried out at the Centre for High Performance Computing in Cape Town.

References

1. Bandichhor, R.; Petrescu, A. D.; Vespa, A.; Kier, A. B.; Schroeder, F.; Burgess, K. *J. Am. Chem. Soc.* **2006**, *128*, 10688–10689.
2. Du, P. W.; Lippard, S. J. *Inorg. Chem.* **2010**, *49*, 10753–10755.
3. Ali, H.; van Lier, J. E. In *Handbook of Porphyrin Science*, Vol. 4; Kadish, K. M.; Smith, K. M.; Guilard, R. Eds. World Scientific: Singapore, 2010, pp. 1–119.
4. Nyokong, T.; Ahsen, V. Eds. *Photochemical and Photophysical Characterization, in Photosensitizers in Medicine, Environment, and Security*; Springer: New York, NY, USA, 2012.
5. Kobayashi, N.; Nakajima, S.; Osa, T. *Inorg. Chim. Acta* **1993**, *210*, 131–133.
6. Kobayashi N.; Nakajima, S.; Ogata, H.; Fukuda, T. *Chem. Eur. J.* **2004**, *10*, 6294–6312.
7. Gorman, A.; Killoran, J.; O'Shea, C.; Kenna, T.; Gallagher, W. M.; O'Shea, D. F. *J. Am. Chem. Soc.* **2004**, *126*, 10619–10631.
8. McDonnell, S. O.; Hall, M. J.; Allen, L. T.; Byrne, A.; Gallagher, W. M.; O'Shea, D. F. *J. Am. Chem. Soc.* **2005**, *127*, 16360–16361.
9. Yogo, T.; Urano, Y.; Ishitsuka, Y.; Maniwa, F.; Nagano, T. *J. Am. Chem. Soc.* **2005**, *127*, 12162–12163.
10. Yang, Y.; Guo, Q.; Chen, H.; Zhou, Z.; Guo, Z.; Shen, Z. *Chem. Commun.* **2013**, *49*, 3940–3942.
11. Lu, H.; Mack, J.; Yang, Y.; Shen, Z. *Chem. Soc. Rev.* **2014**, *43*, 4778–4823.
12. Loudet, A.; Burgess, K. *Chem. Rev.* **2007**, 107, 4891–4932.
13. Lu, H.; Shimizu, S.; Mack, J.; You, X. Z.; Shen, Z.; Kobayashi, N. *Chem. Asian J.* **2011**, *6*, 1026–1037.
14. Liu, H.; Mack, J.; Guo, Q.; Kobayashi, N.; Shen, Z. *Chem. Commun.* **2011**, *47*, 12092–12094.
15. Mack, J.; Asano, Y.; Kobayashi, N. Stillman, M. J. *J. Am. Chem. Soc.* **2005**, *127*, 17697–17711.
16. Michl, J. *J. Am. Chem. Soc.* **1978**, *100*, 6801–6811.
17. Michl, J. *J. Am. Chem. Soc.* **1978**, *100*, 6812–6818.
18. Michl, J. *Pure Appl. Chem.* **1980**, *52*, 1549–1563.
19. Michl, J. *Tetrahedron* **1984**, *40*, 3845–3934.
20. Magyar, R. J.; Tretiak, S. J. *J. Chem. Theory Comput.* **2007**, *3*, 976–987.
21. Cai, Z. L.; Crossley, M. J.; Reimers, J. R.; Kobayashi, R; Amos, R. D. *J. Phys. Chem. B* **2006**, *110*, 15624–15632.
22. Nemykin, V. N.; Hadt, R. G.; Belusludov, R. V.; Mizuseki, H.; Kawazoe Y. *J. Phys. Chem. A* **2007**, *111*, 12901–12913.
23. Gouterman, M. In *The Porphyrins*, Vol. 3, Part A; Dolphin, D. Ed. Academic Press: New York, NY, USA, 1978, pp. 1–165.
24. Lash, T. D. *J. Porphyrins Phthalocyanines* **2001**, *5*, 267–288.
25. Xu, H. J.; Mack, J.; Descalzo, A. B.; Shen, Z.; Kobayashi, N.; You, X. Z.; Rurack, K. *Chem. Eur. J.* **2011**, *17*, 8965–8983.
26. Xu, H. J.; Mack, J.; Wu, D.; Xue, Z. L.; Descalzo, A. B.; Rurack, K.; Kobayashi, N.; Shen, Z. *Chem. Eur. J.* **2012**, *18*, 16844–16867.

27. Blackburn, E. V.; Timmons, C. J. *J. Chem. Soc. C* **1970**, 175–178.
28. Cammidge, A. N.; Gopee, H. *Chem. Eur. J.* **2006**, *12*, 8609–8613.
29. Cammidge, A. N.; Gopee, H. *Chem. Commun.* **2002**, 966–967.
30. Galpern, M. G.; Luk'yanets, E. A. *Zh. Obshch. Khim.* **1969**, *39*, 2536–2541.
31. Galpern, M. G.; Luk'yanets, E. A. *Zh. Obsch. Khim.* **1971**, *41*, 2549–2552.
32. Kudrevich, S.V.; van Lier, J. E.; Galpern, M. G.; Luk'yanets, E. A. *Can. J. Chem.* **1996**, *74*, 508–515.
33. Kudrevich, S.V.; van Lier, J. E. *Can. J. Chem.* **1996**, *74*, 1718–1723.
34. Kopecky, K.; Novakova, V.; Miletin, M.; Kučera, R.; Zimcik, P. *Bioconjugate Chem.* **2010**, *21*, 1872–1879.
35. Kopecky, K.; Novakova, V.; Miletin, M.; Kučera, R.; Zimcik, P. *Tetrahedron* **2011**, *67*, 5956–5963.
36. Zimcik, P.; Novakova, V.; Kopecky, K.; Miletin, M.; Zeynep, R.; Kobak, U. *Inorg. Chem.* **2012**, *51*, 4215–4223.
37. Novakova, V.; Miletin, M.; Filandrová, T.; Lencŏ, J.; R̊užička, A.; Zimcik, P. *J. Org. Chem.* **2014**, *79*, 2082–2093.
38. Faust, R.; Weber, C. *J. Org. Chem.* **1999**, *64*, 2571–2573.
39. Löser, P.; Winzenburg, A.; Faust, R. *Chem. Commun.* **2013**, *49*, 9413–9415.
40. Engelhardt, V.; Kuhri, S.; Fleischhauer, J.; García-Iglesias, M.; González-Rodríguez, D.; Bottari, G.; Torres, T.; Guldi, D. M.; Faust, R. *Chem. Sci.* **2013**, *4*, 3888–3893.
41. Rusanova, J.; Pilkington, M.; S. Decurtins, S. *Chem. Commun.* **2002**, 2236–2237.
42. Rio, Y.; Seitz, W.; Gouloumis, A.; Vázquez, P.; Sessler, J. L.; Guldi, D. M.; Torres, T. *Chem. Eur. J.* **2010**, *16*, 1929–1940.
43. Göl, C.; Malkoç, M.; Yeşilot, S.; Durmuş, M. *Dalton Trans.* **2014**, *43*, 7561–7569.
44. Göl, C.; Malkoç, M.; Yeşilot, S.; Durmuş, M. *Dyes Pigments* **2014**, *111*, 81–90.
45. Frisch, M. J.; Trucks, G. W.; Schlegel, H. B.; Scuseria, G. E.; Robb, M. A.; Cheeseman, J. R.; Scalmani, G.; Barone, V.; Mennucci, B.; Petersson, G. A. et al. Gaussian 09, Revision D.01; Gaussian, Inc.: Wallingford, CT, USA, 2009.
46. Eisner, U.; Linstead, R. P. *J. Chem. Soc.* **1955**, 3749–3754.
47. Gouterman, M. *J. Mol. Spectrosc.* **1961**, *6*, 138–163.
48. Kopranenkov, V. N.; Daskevich, S. N.; Luk'yanets, E. A. *Zh. Obsch. Khim.* **1979**, *49*, 1408–1412.
49. Yamada, H.; Kuzuhara, D.; Takahashi, T.; Shirnizu, Y.; Uota, K.; Okujima, T.; Uno, H.; Ono, N. *Org. Lett.* **2008**, *10*, 2947–2950.
50. Novak, B. H.; Lash, T. D. *J. Org. Chem.* **1998**, *63*, 3998–4010.
51. Linstead, R. P.; Whalley, M. *J. Chem. Soc.* **1952**, 4839–4846.
52. Whalley, M. *J. Chem. Soc.* **1961**, 866–869.
53. Kobayashi, N.; Mack, J.; Ishii, K.; Stillman, M. J. *Inorg. Chem.* **2002**, *41*, 5350–5363.